RSC Advances

This article can be cited before page numbers have been issued, to do this please use: S. Gu, Y. Chen, X. Yuan, H. Wang, X. Chen, Y. Liu, Q. Jiang, Z. Wu and G. Zeng, *RSC Adv.*, 2015, DOI: 10.1039/C5RA16114B.

ROYAL SOCIETY
OF CHEMISTRY

www.rsc.org/advances

View Article Online
DOI: 10.1039/C5RA16114B

Facile synthesis of CeO_2 nanoparticles sensitized CdS nanorods photocatalyst with improved visible-light photocatalytic degradation of Rhodamine B

Shansi Gu [a, b], Yaoning Chen [a, b] *, Xingzhong Yuan [a, b, c]**, Hou Wang [a, b], Xiaohong Chen [c], Yang Liu [a, b], Qian Jiang [a, b], Zhibin Wu [a, b], Guangming Zeng [a, b]

[a] College of Environmental Science and Engineering, Hunan University, Changsha 410082, PR China

[b] Key Laboratory of Environment Biology and Pollution Control, Hunan University, Ministry of Education, Changsha 410082, PR China

[c] Collaborative Innovation Center of Resource-conserving & Environment-friendly Society and Ecological Civilization, Changsha 410083, PR China

---

* Corresponding author at: College of Environmental Science and Engineering, Hunan University, Changsha 410082, PR China. Tel.: +86 73188821413; fax: +86 73188821413
E-mail address: cyn@hnu.edu.cn (Y.N. Chen)
** Corresponding author at: College of Environmental Science and Engineering, Hunan University, Changsha 410082, PR China. Tel.: +86 73188821413; fax: +86 731 88823701.
E-mail address: yxz@hnu.edu.cn (X.Z. Yuan)

View Article Online
DOI: 10.1039/C5RA16114B

Abstract： A heterostructures photocatalyst consisting of one-dimensional (1D) CdS nanorods (NRs) and cerium dioxide (CeO_2) nanoparticles (NPs) were successfully synthesized via a solvothermal method. Different characterization techniques confirmed that CeO_2 NPs were intimately attached on CdS NRs. The visible-light-driven photocatalytic activity was evaluated by the discoloration of Rhodamine B (RhB). It was indicated that, under visible light illumination, the photocatalytic rate constant of CdS/CeO_2 was nearly 3.4 times and 28 times higher than that of pure CdS and pure CeO_2, respectively, owing to the high oxygen storage capacity of CdS/CeO_2 heterostructure, and the inhibition of electron–hole pair recombination benefited from efficient electron transfer from CdS NRs to CeO_2 NPs. In addition, degradation mechanism of RhB on CdS/CeO_2 was also discussed. This durable nanocomposite catalyst, with its excellent combination of CdS NRs and CeO_2 NPs, is able to be a promising catalyst for RhB degradation under visible-light irradiation.

Keywords: CdS/CeO_2 heterostructures; visible-light photocatalysis; Rhodamine B;

View Article Online
DOI: 10.1039/C5RA16114B

1. Introduction

Photocatalytic degradation of pollutants through semiconductor compounds has become a promising approach to solve environmental problems during the last few decades. Among all semiconducting nanostructures, one-dimensional (1D) nanostructures have captured particular attention. At first, 1D geometry can result in a fast and long-distance electron transport. Moreover, their high length-to-diameter ratio can enhance the light absorption and scattering. At last, 1D structures own larger specific surface area that cannot be obtained in their bulk counterparts[1-4].

Metal chalcogenides, such as CdS[5], ZnS[4]， CuS[6]， In_2S_3[7] and SnS_2[8], have been received growing attention on account of their suitable band gap which belongs to the visible spectrum. Among these, CdS, with a direct band gap of 2.4 eV, has been extensively investigated in numerous applications, such as gas sensers[9], lasing[10] and waveguide material[11], solar cell[12], environment purification[13] and hydrogen evolution[3, 14], owing to its relatively high ability in harvesting visible light, favorable conduction band potential and inexpensive cost[14, 15]. However, the quick recombination of photo-generated charge carriers and the serious photocorrosion property are two major defects existing in the CdS catalyst[14]. In order to solve these problems, different strategies included element doping[16], fabricating nano-scaled CdS of different geometric shapes (i.e. rings[10], belts[17], tubes[18] and rods[19]) and sensitization with other metal oxides[14, 19] have been adopted. Particularly, heterostructures photocatalyst composed of CdS NRs and metal oxides opens up a new window to construct high-quality and high-efficiency visible-light-driven photocatalysts[14, 19, 20]. Khan *et al.*[14] reported a hierarchical three-dimensional NiO-CdS heteroarchitecture, which showed an ultra-high photocatalytic activity for hydrogen generation. The enhanced hydrogen production rate was mainly ascribed to the enlarged specific surface area and reduction of the recombination rate of electron–hole pairs. Moreover, 1D CdS/α-Fe_2O_3 nanostructures possessed higher activity than CdS NRs for photocatalytic degradation of Methylene Blue under visible-light illumination[13]. On the other hand, earth metal oxides, such as La_2O_3[21], Pr_6O_{11}[22] and CeO_2[23], are usually chosen as co-catalysts to decorate other semiconductors for the fabrication of heterstructure photocatalysts. Among all, CeO_2 is considered to be a promising catalyst for catalytic organics degradation benefiting from its UV absorbing ability, high electrical conductivity, extensively documented oxygen storage capacity[23], multiple redox states as well as extended stability[23-26]. It is well established that CeO_2 and its based composites have been explored in water dissociation[27], CO oxidation[28] , pollutants degradation[29], hydrodenitrogenation[30] and hydrogen production[31]. Accordingly, sensitization titanium dioxide (TiO_2) nanotube array with CeO_2 NPs was conducted. The combination showed largely enhanced charge storage capacity owing to the

View Article Online
DOI: 10.1039/C5RA16114B

increased number of surface active sites induced by the CeO_2 NPs[25]. To the best of our knowledge, there is no report concerning the synthesis of CeO_2 nanoparticles sensitized CdS nanorods heterstructures photocatalyst for the application of dye degradation.

In this work, we demonstrated the photocatalytic degradation of Rhodamine B under visible light illumination using a novel CdS nanorods/CeO_2 nanoparticles heteroarchitecture fabricated by a facile hydrothermal route. The degradation mechanism of RhB dyes on CdS/CeO_2 was proposed.

2. Experimental

For the sample preparation, characterization and photocatalytic test have been shown in the Experimental section in the Supporting Information.

3. Results and discussions

3.1. FE-SEM and TEM images

The detailed morphology and size of the synthesized products were visualized by SEM and TEM. As shown in Fig. 2a, the highly ordered CdS NRs displayed an average rod diameter of about 100 nm with a length of 1–2 μm. From Fig. 2b and 2c, it can be found that the CeO_2 NPs with an average diameter around 12 nm were anchored on the wall of the CdS NRs. Acting as a “spacer”, the CeO_2 NPs on CdS NRs can prevent the CdS NRs from aggregation[32]. HRTEM measurements were

View Article Online
DOI: 10.1039/C5RA16114B

further performed to investigate the detailed shape and crystal facets of the CdS/CeO_2 heterostructure. As demonstrated in Fig. 2e, the different orientation and lattice fringe of CdS NRs and CeO_2 NPs can be clearly observed. One interplanar distances of 0.34 nm can be indexed to the (002) direction of hexagonal CdS (d = 0.336 nm). The crystallite attached to the CdS with d-spacing of 0.315 nm matched well with the crystal facet (111) of cubic CeO_2. The presence of integration interface between CdS (002) and CeO_2 (111) further confirmed the strong interaction between CdS and CeO_2 in CdS/CeO_2.

3.2. X-ray diffraction analysis

XRD patterns of the as-prepared CdS NRs, CeO_2 NPs and CdS/CeO_2 nanocomposite were shown in Fig. 3. It was observed that the phase of CdS/CeO_2 samples was composited of cubic structure of CeO_2 (JCPDS 43-1002) and hexagonal structure of CdS (JCPDS 41-1049). For CdS NRs, the characteristic peaks at 2θ values of 24.8°, 26.5°, 28.2°, 43.7°, 47.8° and 70.8° can be indexed to the (100), (002), (101), (110), (103) and (211) planes of hexagonal wurtzite crystal structured CdS NRs, respectively. The peaks of cubic fluorite structured CeO_2 at 33.1°, 56.3° and 69.4° were originated from the (200), (311) and (400) diffractions, respectively. Though some crystal plane diffraction peaks of CeO_2 may overlapped with the peaks of CdS, two main peaks {(200) and (311)} of CeO_2 appeared in the XRD profiles of

View Article Online
DOI: 10.1039/C5RA16114B

CdS/CeO_2 confirmed the existence of CeO_2 NPs on CdS NRs.

3.3. X-ray photoelectron spectroscopy (XPS) analysis

To investigate the chemical and oxidation states for Cd, S, Ce and O, XPS analysis was carried out. The spin–orbit components ($3d^{5/2}$ and $3d^{3/2}$) of the Cd 3d peak were well deconvoluted for CdS/CeO_2 nanocomposites by two curves at approximately 411.93 eV and 405.17 eV (Fig. 4a), manifesting that cadmium was in the Cd^{2+} state in the samples[15]. Meanwhile, the determined binding energies of S 2p were found located at 161.51 eV and 162.7 eV (Fig. 4b), corresponding to sulfide species (S^{2-}) of CdS/CeO_2 composites[5]. Fig. 4c showed the profile of high resolution XPS spectra of Ce 3d in CdS/CeO_2 composites. It was found that a small amount of Ce^{3+} (885.4 and 904.1 e V) were coexisting with Ce^{4+} (882.1 eV, 888.9 eV, 898 eV, 900.3 eV, 907.6 eV and 916.6 eV) in the nanocomposites[28]. By fitting the curves and calculating the $Ce^{3+}/(Ce^{3+} + Ce^{4+})$, a pronouncedly high Ce^{3+} ratio of 20.5% on CdS/CeO_2 was identified, which was higher than that of CeO_2/graphene (18.5%) reported in earlier study[33]. Usually, Ce^{3+} content is proportional to oxygen vacancies, the utra-high Ce^{3+} ratio denote that a certain amount of oxygen vacancies were introduced in the nanocomposites[34]. This result was further confirmed by the XPS result of the O 1s region depicted in Fig. 4d. The O 1s spectrum was matched with three peaks at 529.12 eV, 531.94 eV and 533.68 eV. The distinct shoulder detected at

View Article Online
DOI: 10.1039/C5RA16114B

531.94 eV was corresponded to the adsorbed oxygen and weakly bonded oxygen species; the peak with the highest binding energy belonged to oxygen by hydroxide or adsorbed water on the catalyst surface. Both of the peaks illustrated above confirmed the existent of plenty of surface oxygen vacancies in CdS/CeO_2. Meanwhile, the weakest peak, located at 529.12 eV, was found attributed to lattice oxygen in the anchored CeO_2 nanocrystals[28, 29, 35]. Generally, surface adsorbed oxygen is more reactive than lattice oxygen in oxidation reactions on account of its higher mobility[35]. Hence, the higher surface adsorbed oxygen amount on CdS/CeO_2 was helpful for the photocatalytic pollutant degradation, leading a significantly enhanced photocatalytic ability of CdS/CeO_2 for the degradation of RhB.

3.4. N_2 adsorption–desorption

The specific surface areas were recorded from the N_2 adsorption-desorption isotherms using the BET analysis method. Fig. 5 showed the nitrogen adsorption-desorption isotherms for pure CdS, CeO_2 and CdS/CeO_2 ($R_C = 20$) compound. Apparent hysteresis loops can be distinguished on the adsorption–desorption isotherms of CdS nanorods, CeO_2 nanoparticles and CdS/CeO_2, indicating the existence of porous structures. The surface area data are summarized in Table 1. As we can see, the total pore volume of CdS/CeO_2 is increased a lot, which may come from the voids between the aggregated CeO_2 particles and CdS rods. Besides, the

View Article Online
DOI: 10.1039/C5RA16114B

surface area increased by addition of CeO_2 to CdS. For the pristine CdS nanorod, a specific surface area of 13.1 m^2/g was obtained, whereas for CdS/CeO_2 sample (R_C = 20), the specific surface area was 21.8 m^2/g. The higher BET surface area for CdS/CeO_2 nanocomposites was presumed to result from the CeO_2 NPs (24 m^2/g) linked on CdS NRs depressed the agglomeration of CdS NRs. Consequently, the increased surface area might be one of the reasons responsible for the enhanced photocatalytic activity.

3.5. UV–vis diffuse reflectance spectroscopy analysis

The Ultraviolet–visible (UV–vis) diffuse reflectance spectroscopy was employed to measure the optical properties of the samples. The corresponding absorption spectra of CdS, CeO_2 and CdS/CeO_2 (Rc = 20) were displayed in Fig. 6. It was obvious that CdS/CeO_2 nanocomposite exhibited a CdS absorption peak and a feature band edge of individual CeO_2. Compared with pristine CdS and CeO_2, CdS/CeO_2 appeared spectral response in a broader visible-light region ascribed to the photosentisizing effect of CeO_2. According to the following equation:

$$(\alpha h v)^n = \mathrm{A}(h v - \mathrm{E_g}) \tag{1}$$

Where α is the absorption coefficient, v is the light frequency, A is a constant, E_g is the band gap energy, and n is 1/2 and 2 for CdS and CeO_2, respectively. The E_g of the as-prepared samples can be calculated from a plot depicting $(\alpha hv)^n$ versus (hv) (shown

View Article Online
DOI: 10.1039/C5RA16114B

in Fig S2). The extrapolated values (the straight line to the *x* axis) of *(hv)* at α=0 gives absorption edge energies consistent with E_g = 2.37 eV and E_g = 2.95 eV for CdS and CeO_2, respectively.

3.6. Photocatalytic activity

3.6.1. Effect of the amount of CeO_2 nanoparticles loading on CdS nanorods

Decomposition of RhB (C_0 = 40 mg/L) under the identical conditions was carried out to determine the activities of samples with different molar ratio. The UV-vis spectral change of CdS-CeO_2/RhB dispersion after 60 min adsorption in the dark was depicted in Fig. S3. It was clear that no wavelength shift of the band at 554 nm was observed, indicating RhB was not decomposed during the dark reaction. The decreased absorbency of CdS-CeO_2/RhB dispersion was corresponding to the extent of RhB adsorption on CdS/CeO_2. The results of RhB degradation over CdS, CeO_2 and CdS/CeO_2 photocatalysts were shown in Fig. 7. It was noticeable that direct visible light irradiation of the RhB dye solution in the absence of catalysts was inconsequential toward degrading the dye. The photoactivity of the sample was strongly dependent on the R_C value. With R_C increasing from 0 to 20, the photoactivity of the sample for the RhB photodegradation was enhanced. The maximum degradation efficiency reached to 96.68% after 48 min for the sample (R_C = 20). However, when R_C further increased to 30, the photoactivity of the sample

View Article Online
DOI: 10.1039/C5RA16114B

decreased instead. As expected, all samples showed higher photoactivities for the RhB degradation than that of pure CdS and CeO_2 under visible light ($\lambda \geq 420$ nm). Kinetics of the photocatalytic degradation of RhB was a pseudo-first-order[36], which can be explained in the Langmuir-Hinshelwood model:

$$- \ln (C_t/C_0) = kt \qquad (2)$$

The apparent rate constant (k) for the degradation of RhB on these samples were calculated by plotting $\ln(C_0/C_t)$ versus t (Fig. 8), and the results were shown in Table 2. The excellent photocatalytic performances of CdS/CeO_2 heterostructure for RhB degradation may be due to that (i) high oxygen storage capacity of CeO_2 provided immense sources of active species; (ii) the strong interactions between CdS and CeO_2 effectively prevented the photo-corrosion and leaching of CdS; and (iii) effective charge separation reduced the recombination rates of electron-hole pairs. The influence on RhB degradation was also investigated and displayed in the Supporting Information.

3.6.2. Analyses of Intermediate Products.

The temporal evolution of the spectral changes during the photodegradation of RhB over CdS/CeO_2 and CdS were given in Fig. 9a and 9b. It was noteworthy that original RhB depicted a major absorption band at 554 nm, and no shift of the adsorption band was observed after dark reaction for 1h and visible light illumination

View Article Online
DOI: 10.1039/C5RA16114B

for 48 min (Fig. S4). In the presence of CdS, the absorption peak of RhB solution decreased slowly and the absorption band shifted from 554 to 548 nm within 48 min irradiation. By contrast, absorbance of the absorption peak at 554 nm decreased rapidly to almost zero and the wavelengths of the characteristic peaks shifted from 554 nm to 500 nm as the photodegradation reaction proceeded in the presence of CdS/CeO_2. Obviously, hypsochromic shifts of the absorption maximum observed with CdS/CeO_2 suspension were more pronounced than those observed with the CdS system. These hypsochromic shifts were assumed to result from the formation of a series of N-deethylated intermediates of RhB in a stepwise manner and the cleavage of the conjugated chromophore structure[21, 37, 38]. To comprehend the photocatalytic degradation process better, intermediates of RhB during the photodegradation were further confirmed by HPLC monitoring equipped with a UV-visible diode array detector. The HPLC chromatogram of 0, 8, 16, 24, 32, 40 and 48 min filtrate of RhB/CdS-CeO_2 ($R_C = 20$) system were illustrated in Fig. 9c. The maximum concentration of RhB might appeared at the retention time of 4.42 min (peak a). Four other peaks (Fig. 9c, peak b–e), which may belong to N-de-ethylated intermediates, namely, N,N-diethyl-N'-ethylrhodamine (DER), N,N-diethylrhodamine (DR), N-ethyl- N'-ethylrhodamine (EER), N-ethylrhodamine (ER) or Rhodamine (R) were also observed[37, 38]. With the quick diminishing of RhB, the concentration of other N-

View Article Online
DOI: 10.1039/C5RA16114B

deethylated intermediates increased successively and subsequently decreased in succession with further irradiation, which revealed that the N-deethylation of RhB was a stepwise course. It was found that the first N-deethylated intermediate reached its maximum concentration after 16 min irradiation, whereas the final N-deethylated product got disappeared after 40 min irradiation. Based on these results, it was concluded that the RhB was effectively decomposed rather than merely bleached during the CdS/CeO$_2$-assisted photodegradation. The fragmentation pathway of RhB photocatalytic degradation under visible light irradiation in CdS/CeO$_2$ suspension was tentatively proposed as depicted in Fig. 10. Moreover, the total organic carbon (TOC) values of the solution at different time intervals during the RhB degradation was measured (Fig. S5). After 48 min of irradiation, a relatively high mineralization rate of 86% of TOC removal was achieved, indicating that RhB has been mineralized efficiently under visible light irradiation.

3.6.3. Recycle test

To probe the practical reusability of the CdS/CeO$_2$ catalyst in the decomposition of RhB, recycling tests were carried out by repeated reaction cycles under the same reaction condition. As shown in Fig. 11, the catalytic activity of CdS/CeO$_2$ did not significantly decrease after six continuous cycles, in which the RhB removal efficiencies of CdS/CeO$_2$ (Rc = 20) were all above 90%. In sharp contrast, RhB

View Article Online
DOI: 10.1039/C5RA16114B

removal efficiency of pure CdS for the first-cycle test was about 64%, and then obvious deactivation can be observed on CdS after four times recycles, indicating that the CdS/CeO_2 owned a superior reusability in RhB degradation. To further demonstrate the stability of the catalyst, leaching of cadmium from CdS/CeO_2 in solution after six cycle test was measured by via a Perkin-Elmer Analyst 700 atomic absorption spectrophotometer. For comparison, Cd content in solution after four cycle test for CdS catalyst was also detected. Results (inset of Fig. 11) indicated that the Cd ions released rapidly from CdS solid into the solution, which should be resulted from CdS photocorrosion. As for CdS/CeO_2, rather low Cd species in CdS/CeO_2 leached off even after being used six successive times. Moreover, there is no distinction between the XRD results of CdS/CeO_2 samples before and after the reaction (Fig. S6), suggesting its structural stability during the photocatalytic oxidation of the pollutant molecules. The improved stability of CdS/CeO_2 may be ascribed to the intimate interfacial interaction[39, 40] between CdS and CeO_2 and the introducing of high thermal stability CeO_2.

3.6.4. The proposed mechanism of RhB photodegradation

In order to determine the main active species responsible for the degradation of RhB over the optimum CdS/CeO_2 composite ($R_C = 20$), controlled photoactivity experiments were performed with adding different radical scavengers (0.1 mmol) at

View Article Online
DOI: 10.1039/C5RA16114B

the natural pH of the dye. Fig. 12 reflected the photocatalytic activities of CdS/CeO_2 ($R_C = 20$) for the degradation of RhB in the presence of different radical scavengers, i.e., Ethylene Diamine Tetraacetic Acid (EDTA) scavenger for h^+[41], isopropyl alcohol (IPA) for •OH and benzoquinone (BQ) for $O_2•^-$, respectively. It was apparent that the order of affecting the rate for degradation of RhB followed that of $O_2•^- > h^+ >$ •OH. It was shown that significant suppressing effect was obtained after addition of BQ ($O_2•^-$ quencher), suggesting the superoxide anion radical was the major oxidative species responsible for the photooxidative conversion of RhB[36, 42]. The band edge positions of the CB and VB of CdS and CeO_2 was determined according the following equations:

$$E_{VB} = X - E^e + 1/2E_g \tag{3}$$

$$E_{CB} = E_{VB} - E_g \tag{4}$$

Where X is the absolute electronegativity of the semiconductor (X is 5.18 eV and 5.57 eV for CdS and CeO_2, respectively), E^e is the energy of free electrons on the hydrogen scale (4.5 eV) and E_g is the band gap of the semiconductor[26]. The calculated CB and VB of CdS were -0.505 and 1.865 eV, respectively, which were more negative than those of CeO_2 (-0.405 and 2.545 eV, respectively). The standard redox potential of $O_2/ O_2•^-$ and $•OH/OH^-$ is -0.33 and 2.38 V vs NHE[42], respectively. That is, the CB potentials of CeO_2 and CdS were both negative than the standard redox potential of $O_2/ O_2•^-$, whereas the standard redox potential of $•OH/ OH^-$ was positive to the VB of

View Article Online
DOI: 10.1039/C5RA16114B

CdS. As a result, the photogenerated electrons on irradiated CdS/CeO_2 heterostructure can reduce O_2 to give $O_2\bullet^-$, while the photogenerated holes can hardly oxidize OH to give •OH, therefore $O_2\bullet^-$ was the protagonist in RhB photodegradation by CdS/CeO_2. Meanwhile, colorless organic molecules which do not absorb in visible regions were usually used for the evaluation of photocatalytic activity of photocatalyst[36,42-44]. Therefore, colorless bisphenol A (BPA) and salicylic acid (SA) were chosen as the target pollutants. Prior to irradiation, the suspension was stirred for 1 h in dark to reach adsorption–desorption equilibrium. The sample was then irradiated with visible light with continuous stirring. After 1 h irradiation, the BPA and SA removal ratio of CdS/CeO_2 (Rc = 20) was 31.4% and 46.3%, respectively. While the pure CdS showed a degradation ratio of 5.2% and 7.7%, for BPA and SA, respectively. Therefore, it was suggested that the CdS/CeO_2 composites is indeed a visible-light induced photocatalyst. Besides, considering the redox potential of $E^0_{RhB^*/RhB\bullet+}$(−1.09 V vs. SHE) and $E^0_{RhB\bullet+/RhB}$ (1.46 V vs. SHE)[42], photo-induced electrons can transfer from photoexcited dye (RhB*) to the conduction bands of CdS, which has also been reported by Takuo et al[45, 46]. Based on the above discussion, a tentative illustration of possible interparticle electron transfer behavior can be proposed, as illustrated in Fig. 13. Under visible-light irradiation, photo-induced electrons easily transferred from photoexcited dye (RhB*) to the CB of CdS to form $RhB^{+\bullet}$. These transferred electrons

View Article Online
DOI: 10.1039/C5RA16114B

captured by adsorbed oxidants to generate active species (e.g., $O_2^{\bullet-}$). Afterwards, RhB+• could be consumed by these generated $O_2^{\bullet-}$ radicals. On the other hand, the electrons could be photoexcited directly from the VB of CdS NRs to the CB of CdS by adsorbing light, forming electron-hole pairs. Immediately, the generated electrons of CdS transferred to the CB of CeO_2. After that, the transferred electrons trapped by the adsorbed oxygen on the surface of the catalyst to produce reactive oxygen radicals ($O_2\bullet^-$). Finally, RhB dyes adsorbed on the surface of CdS/CeO_2 was attacked by the activated oxygen to decolorize the solution. Simultaneously, holes generated in CdS/CeO_2 can directly react with adsorbed dyes, making contributions to the RhB degradation process. The overall decomposition of RhB can be expressed by the following formula:

$$\mathrm{RhB} + h\nu \rightarrow \mathrm{RhB}^* \quad (5)$$

$$\mathrm{RhB}^* + \mathrm{CdS} \rightarrow \mathrm{RhB}^{\bullet+} + \mathrm{CdS}\ (e^-) \quad (6)$$

$$\mathrm{CdS} + h\nu \rightarrow \mathrm{CdS}\ (e^- + h^+) \quad (7)$$

$$\mathrm{CdS}\ (e^-) + \mathrm{CeO_2} \rightarrow \mathrm{CeO_2}\ (e^-) \quad (8)$$

$$e^-_{(\mathrm{CB,CeO_2})} + \mathrm{O_2} \rightarrow \mathrm{O_2}^{\bullet-} \quad (9)$$

$$\mathrm{RhB/\ RhB}^{\bullet+} + (\mathrm{O_2}^{\bullet-} + h^+) \rightarrow \text{mineralized products} \rightarrow \mathrm{CO_2 + H_2O} \quad (10)$$

4. Conclusions

Nanocomposites made with CdS NRs and CeO_2 NPs were successfully

View Article Online
DOI: 10.1039/C5RA16114B

synthesized using a hydrothermal method. FE-SEM and TEM analyses showed that the CeO_2 NPs were anchored on the wall of the CdS NRs strongly. XPS spectra and XRD result confirmed the formation of CdS/CeO_2 heterostructures. The CeO_2 played a vital role in achieving excellent photocatalytic performance of the synthesized composites toward degradation of RhB due to its large oxygen capacity and facilitation for the electron-hole pair separation. RhB was decomposed around 97% under visible light over CdS/CeO_2, which was much enhanced than original CdS NRs (64%) and CeO_2 NPs (12%). The sample ($R_C = 20$) had the highest kinetic rate constant ($0.07 min^{-1}$) owing to the effective charge separation and excellent redox capacity of photocatalysts. Results also demonstrated that the degradation efficiency increased with decreasing pH values. It is hoped that more ongoing research efforts could be paid to the earth metal oxides and the fabrication of 1D semiconductor nanostructures.

Acknowledgments

This work is supported by the National Natural Science Foundation of China (No. 71431006, 21276069), the State Scholarship Fund and the Fundamental Research Funds for the Central Universities.

References

1. S. Liu, N. Zhang, Z. R. Tang and Y. J. Xu, *ACS. Appl. Mater. Inter.*, 2012, **4**, 6378-

View Article Online
DOI: 10.1039/C5RA16114B

6385.

2. B. Weng, S. Liu, N. Zhang, Z.-R. Tang and Y. J. Xu, *J. Catal.*, 2014, **309**, 146-155.

3. X. Wang, G. Liu, G. Q. Lu and H.-M. Cheng, *Int. J. Hydrogen Energ.*, 2010, **35**, 8199-8205.

4. L. P. Wu, Y. L. Zhang, L. Z. Long, C. P. Cen and X. J. Li, *RSC Adv.*, 2014, **4**, 20716-20721.

5. P. Gao, J. Liu, D. D. Sun and W. Ng, *J. Hazard. Mater.*, 2013, **250-251**, 412-420.

6. Y. Wang, L. Zhang, H. Jiu, N. Li and Y. Sun, *Appl. Surf. Sci.*, 2014, **303**, 54-60.

7. M. Xie, X. Dai, S. Meng, X. Fu and S. Chen, *Chem. Eng. J.*, 2014, **245**, 107-116.

8. X. Yuan, H. Wang, Y. Wu, X. Chen, G. Zeng, L. Leng and C. Zhang, *Catal. Commun.*, 2015, **61**, 62-66.

9. L. Zhu, C. Feng, F. Li, D. Zhang, C. Li, Y. Wang, Y. Lin, S. Ruan and Z. Chen, *RSC Adv.*, 2014, **4**, 61691-61697.

10. Z. Hu, X. Guo and L. Tong, *Appl. Phys. Lett.*, 2013, **103**, 183104.

11. A. Pan, D. Liu, R. Liu, F. Wang, X. Zhu and B. Zou, *Small*, 2005, **1**, 980-983.

12. R. Yang, D. Wang, L. Wan and D. Wang, *RSC Adv.*, 2014, **4**, 22162-22171.

13. Le Wang, Hongwei Wei, Yingju Fan, Xin Gu and J. Zhan, *J. Phys. Chem. C*, 2009, **113**, 14119-14125.

14. Z. Khan, M. Khannam, N. Vinothkumar, M. De and M. Qureshi, *J. Mater. Chem.*,

DOI: 10.1039/C5RA16114B

2012, **22**, 12090-12095.

15. R. C. Pawar and C. S. Lee, *Appl. Catal. B: Environ.*, 2014, **144**, 57-65.
16. J. E. C. AIOLIVA∗, R PATIÑO and A I OLIVA-AVILÉS, *Bull. Mater. Sci.*, 2014, **37**, 247-255.
17. Y. Ye, L. Dai, X. Wen, P. Wu, R. Pen and G. Qin, *ACS Appl. Mate. Inter.*, 2010, **2**, 2724-2727.
18. Y. Xiong, Y. Xie, J. Yang, R. Zhang, C. Wu and G. Du, *J. Mate. Chem.*, 2002, **12**, 3712-3716.
19. C. Luan, T. L. Wong and J. A. Zapien, *J. Cryst. Growth*, 2013, **374**, 65-70.
20. S. Yan, D. Hu, J. Wu, X. Xu, J. Wang and Z. Xiao, *J. Alloy. Compd.*, 2011, **509**, L239-L243.
21. H. Xu, H. Li, G. Sun, J. Xia, C. Wu, Z. Ye and Q. Zhang, *Chem. Eng. J.*, 2010, **160**, 33-41.
22. C. Karunakaran, R. Dhanalakshmi and P. Anilkumar, *Chem. Eng. J.*, 2009, **151**, 46-50.
23. N. Laosiripojana, W. Sutthisripok and S. Assabumrungrat, *Chem. Eng. J.*, 2007, **127**, 31-38.
24. Q. Dai, J. Wang, J. Yu, J. Chen and J. Chen, *Appl. Catal. B: Environ.*, 2014, **144**, 686-693.

View Article Online
DOI: 10.1039/C5RA16114B

25. H. Wen, Z. Liu, Q. Yang, Y. Li and J. Yu, *Electrochim. Acta*, 2011, **56**, 2914-2918.

26. Z.-M. Yang, G.-F. Huang, W.-Q. Huang, J.-M. Wei, X.-G. Yan, Y.-Y. Liu, C. Jiao, Z. Wan and A. Pan, *J. Mater. Chem. A*, 2014, **2**, 1750.

27. D. R. Mullins, P. M. Albrecht, T.-L. Chen, F. C. Calaza, M. D. Biegalski, H. M. Christen and S. H. Overbury, *J. Phys. Chem. C*, 2012, **116**, 19419-19428.

28. Z. Wang, Q. Wang, Y. Liao, G. Shen, X. Gong, N. Han, H. Liu and Y. Chen, *Chemphyschem*, 2011, **12**, 2763-2770.

29. Y.G Wang, B. Li, L.F. Cui, S.F Kang, X. Li and L.H. Zhou, *Appl. Catal. B: Environ.*, 2013, **130-131**, 277- 284.

30. Z. Sun, X. Li, A. Wang, Y. Wang and Y. Chen, *Top. Catalysis*, 2012, **55**, 1010-1021.

31. X.H. Lu, S.L. Xie, T. Zhai, Y.F. Zhao, P. Zhang, Y.L. Zhang, Y.X. Tong, *RSC Adv.*, 2011, **1**, 1207-1210.

32. Z. Ji, X. Shen, M. Li, H. Zhou, G. Zhu and K. Chen, *Nanotechnology*, 2013, **24**, 115603.

33. L. Jiang, M. Yao, B. Liu, Q. Li, R. Liu, H. Lv, S. Lu, C. Gong, B. Zou, T. Cui, B. Liu, G. Hu and T. Wågberg, *J. Phys. Chem. C*, 2012, **116**, 11741-11745.

34. M. Yu, Y.-A. Zhu, Y. Lu, G. Tong, K. Zhu and X. Zhou, *Appl. Catal. B: Environ.*,

View Article Online
DOI: 10.1039/C5RA16114B

2015, **165**, 43-56.

35. W. Shan, F. Liu, H. He, X. Shi and C. Zhang, *Catalysis Today*, 2012, **184**, 160-165.

36. C. S. Pan, H.B Fu, W. Q. Yao and Y. F. Zhu, *J. Phys. Chem. B*, 2005, **109**, 22432-22439.

37. S. Y. Kai Yu, Huan He, Cheng Sun, Chenggang Gu, Yongming Ju, *J. Phys. Chem. A* 2009, **113**, 10024-10032.

38. T. S. Natarajan, M. Thomas, K. Natarajan, H. C. Bajaj and R. J. Tayade, *Chem. Eng. J.*, 2011, **169**, 126-134.

39. X. Gao, H. B. Wu, L. Zheng, Y. Zhong, Y. Hu and X. W. Lou, *Angew. Chem. Int. Ed.*, 2014, **53**, 5917-5921.

40. H. Li, X. He, Z. Kang, H. Huang, Y. Liu, J. Liu, S. Lian, C. H. Tsang, X. Yang and S. T. Lee, *Angew. Chem. Int. Ed.*, 2010, **49**, 4430-4434.

41. Y. Liu, X. Yuan, H. Wang, X. Chen, S. Gu, Q. Jiang, Z. Wu, L. Jiang and G. Zeng, *Rsc Adv.*, 2015, **5**, 33696-33704.

42. W. Li, D. Li, S. Meng, W. Chen, X. Fu and Y. Shao, *Environ. Sci. technol.*, 2011, **45**, 2987-2993.

43. M. Zhang, C. Chen, W. Ma and J. Zhao, *Angew. Chem.*, 2008, **47**, 9730-9733.

View Article Online
DOI: 10.1039/C5RA16114B

44. J. Sun, G. Chen, J. Wu, H. Dong and G. Xiong, *Appl. Catal. B: Environ.*, 2013, **132-133**, 304-314.

45. T.Watanabe, T. Tadashi and K. Honda, *J. Phys. Chem.*, 1977, **81**, 1845-1851.

46. T. Takirawa, T. Watanabe and K. Honda, *J. Phys. Chem.*, 1978, **82**, 1391-1396.

View Article Online
DOI: 10.1039/C5RA16114B

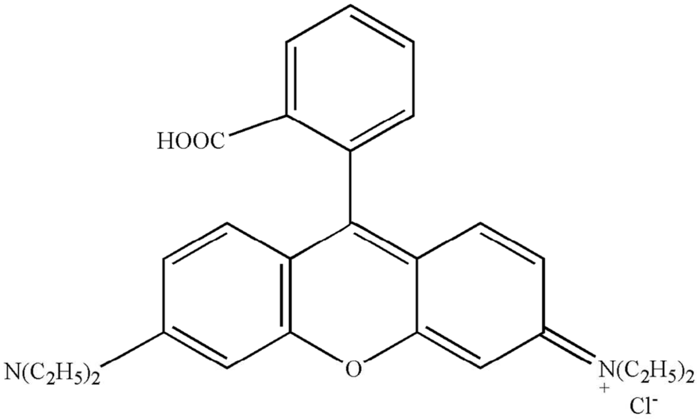

Rhodamine B

Fig. 1. Chemical structure of Rhodamine B.

View Article Online
DOI: 10.1039/C5RA16114B

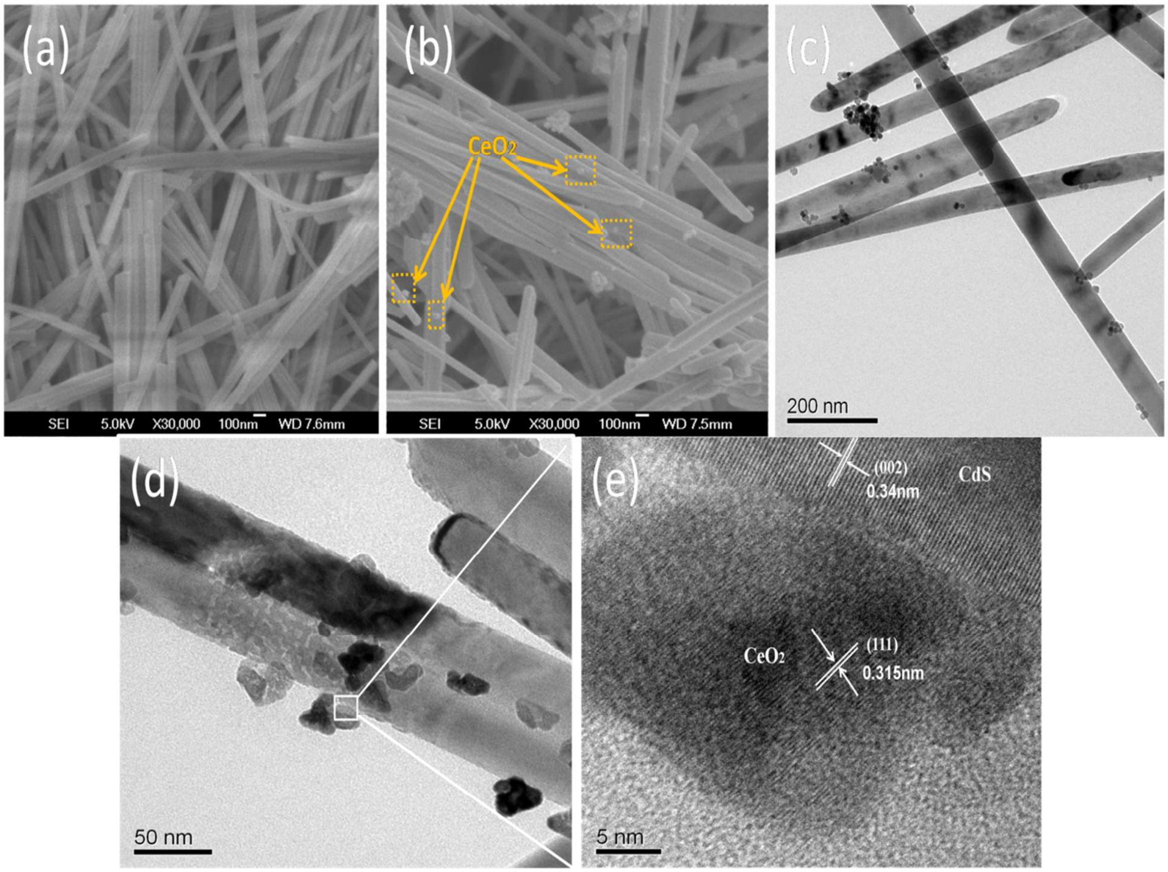

Fig. 2. (a) SEM images of CdS nanorods; (b) SEM image of CdS nanorods decorated with CeO_2 nanoparticles; (c) TEM image of 1D CdS/CeO_2 nanocomposites; (d) Magnified TEM image of CdS/CeO_2 heterostructure; (e) HRTEM images of the rectangular regions.

View Article Online
DOI: 10.1039/C5RA16114B

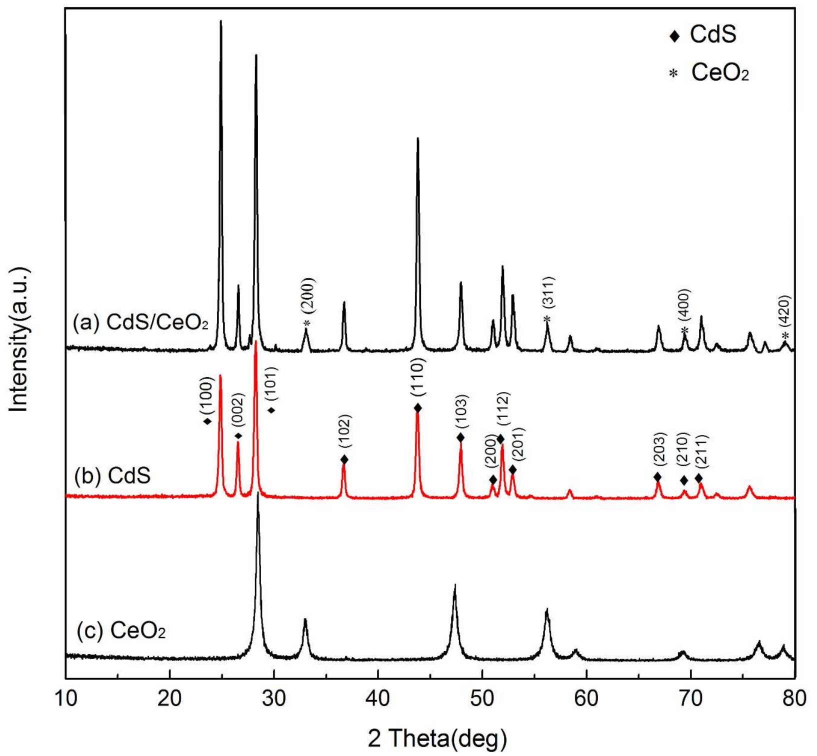

Fig. 3. XRD pattern of CdS/CeO$_2$ nanocomposites (top); CdS nanorods (middle); CeO$_2$ nanoparticles (bottom).

View Article Online
DOI: 10.1039/C5RA16114B

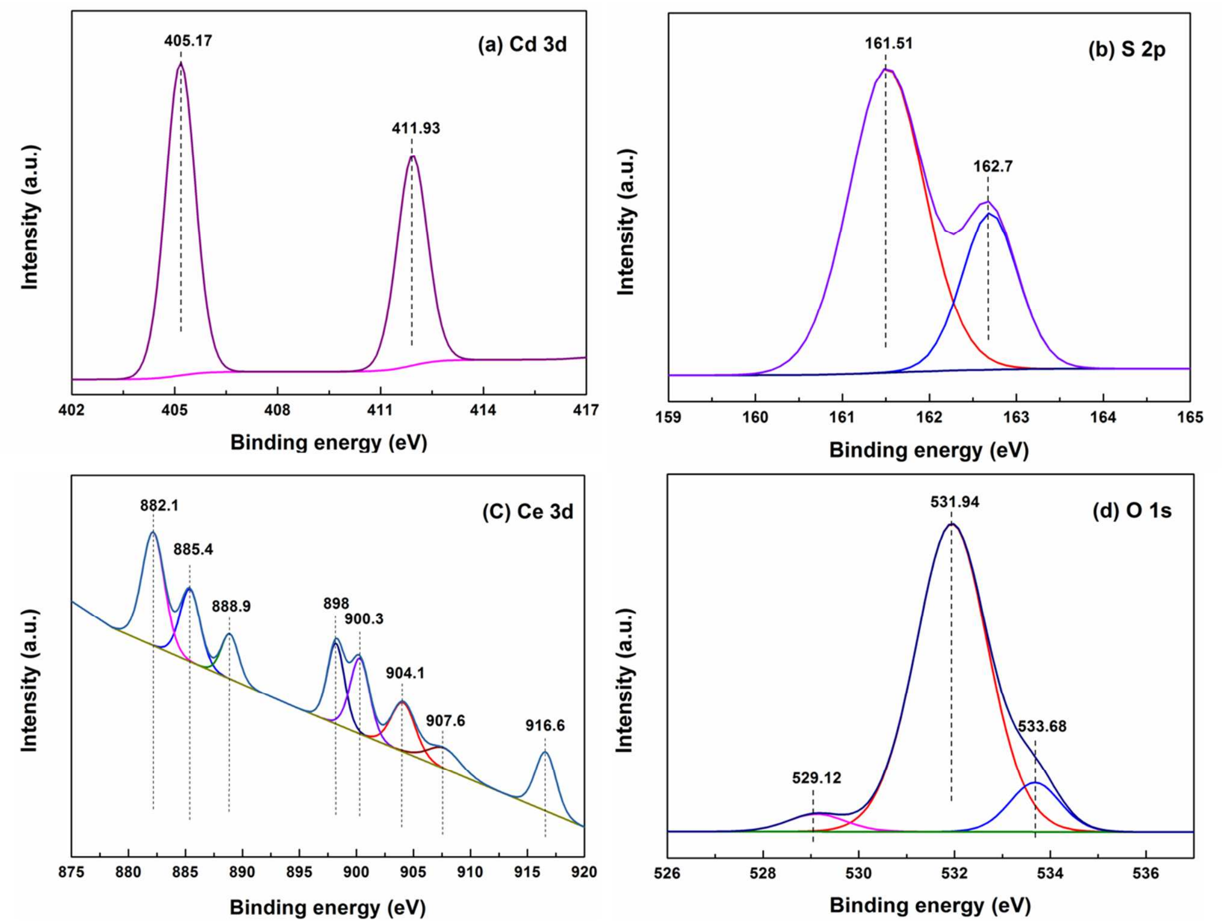

Fig. 4. High-resolution XPS spectrum of the (a) Cd 3d, (b) S 2p, (c) Ce 3d and (d) O 1s.

View Article Online
DOI: 10.1039/C5RA16114B

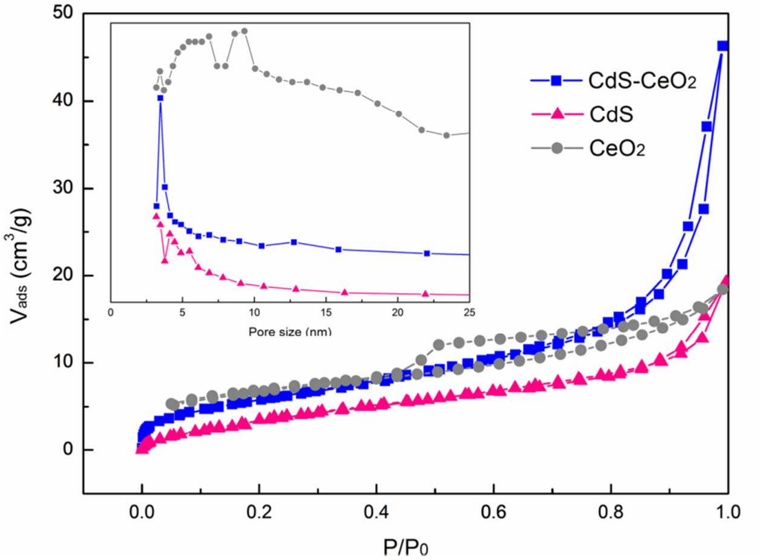

Fig. 5. N_2 adsorption–desorption isotherms for CdS (the magenta line), CeO_2 (the gray line) and CdS/CeO_2 (the blue line). (Inset: the corresponding pore size distribution)

View Article Online
DOI: 10.1039/C5RA16114B

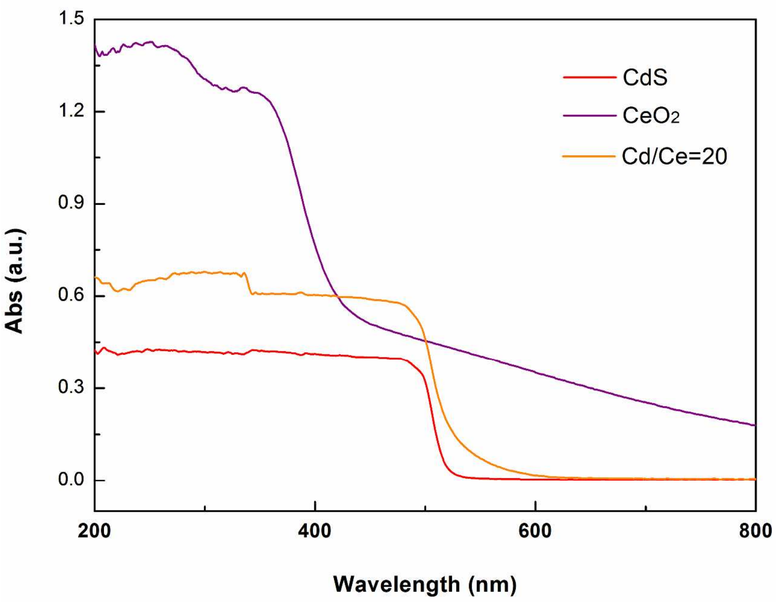

Fig. 6. UV-vis DRS of CdS NRs, CeO_2 NPs and CdS/CeO_2 ($R_C = 20$) heterostructures.

View Article Online
DOI: 10.1039/C5RA16114B

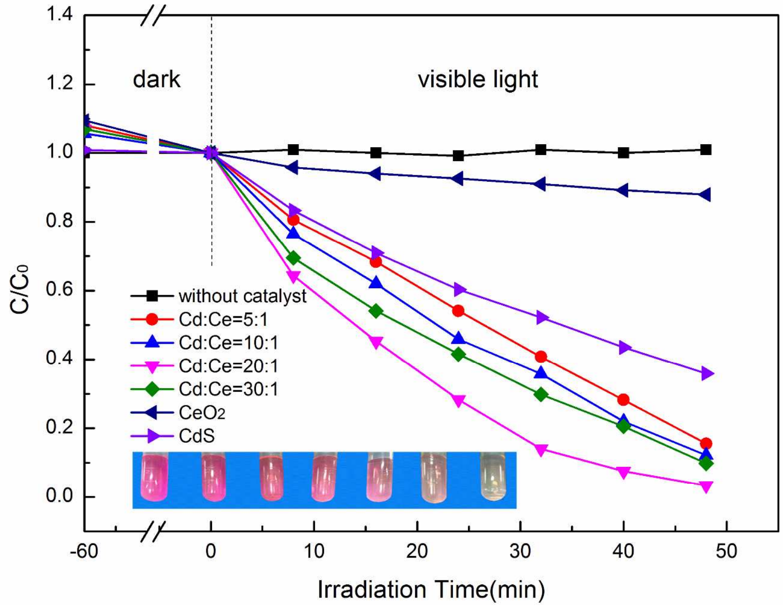

Fig. 7. Effect of CeO_2 loading on photocatalytic degradation of RhB; the suspensions containing 0.4 g/L catalysts, natural pH = 4.3, initial concentration = 40 mg/L, $\lambda \geq 420$ nm.

View Article Online
DOI: 10.1039/C5RA16114B

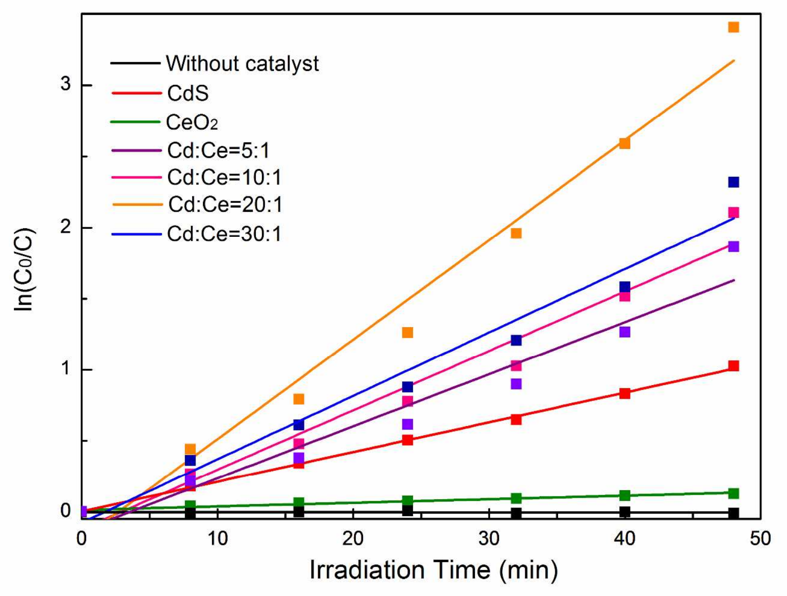

Fig. 8. Kinetic fit for the degradation of RhB with pure CdS, CeO_2 and CdS/CeO_2 catalysts with different CeO_2 contents.

View Article Online
DOI: 10.1039/C5RA16114B

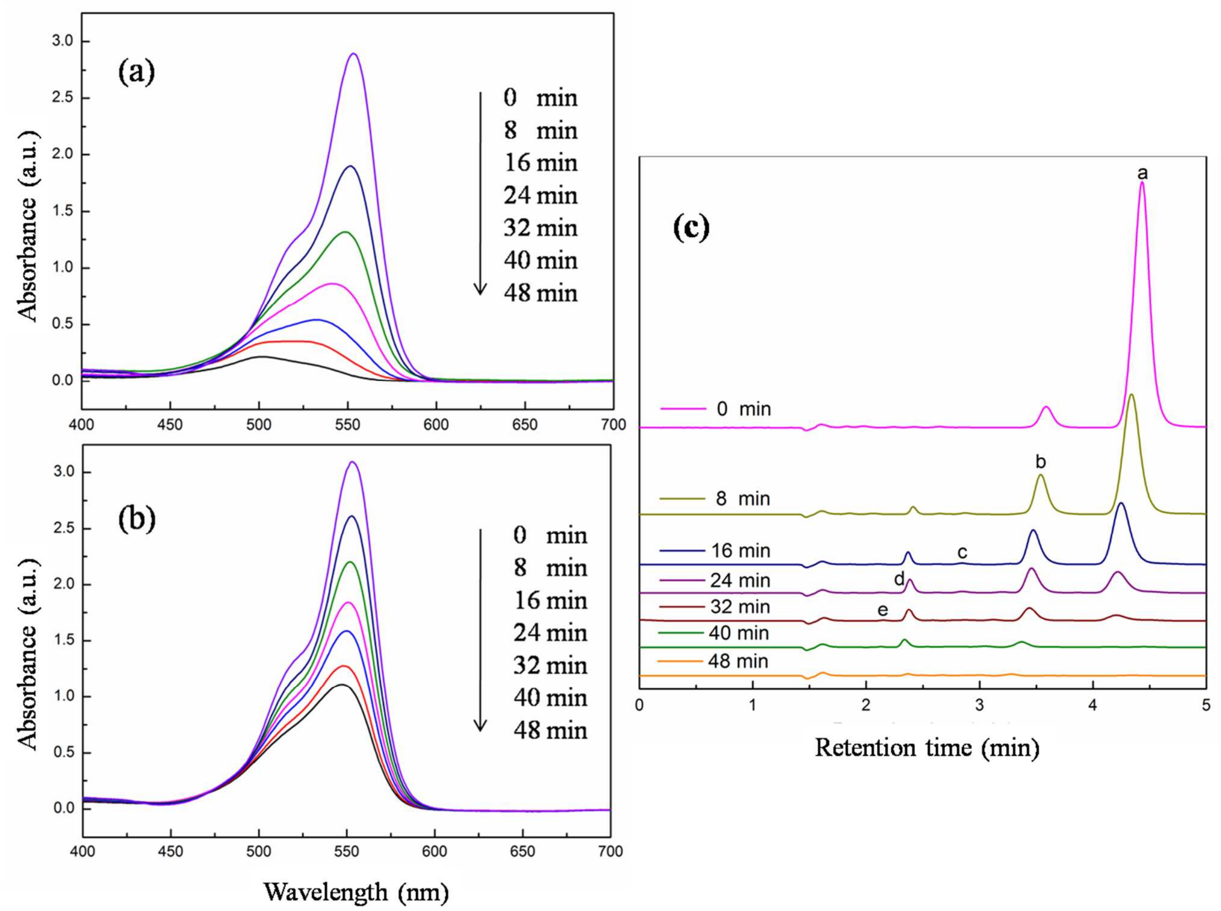

Fig. 9. Temporal spectral changes of RhB in aqueous (a) CeO_2/CdS and (b) CdS dispersion under visible irradiation; (c) HPLC chromatograms of the N-de-ethylated intermediates at different irradiation intervals in the role of CdS/CeO_2 ($R_C = 20$).

View Article Online
DOI: 10.1039/C5RA16114B

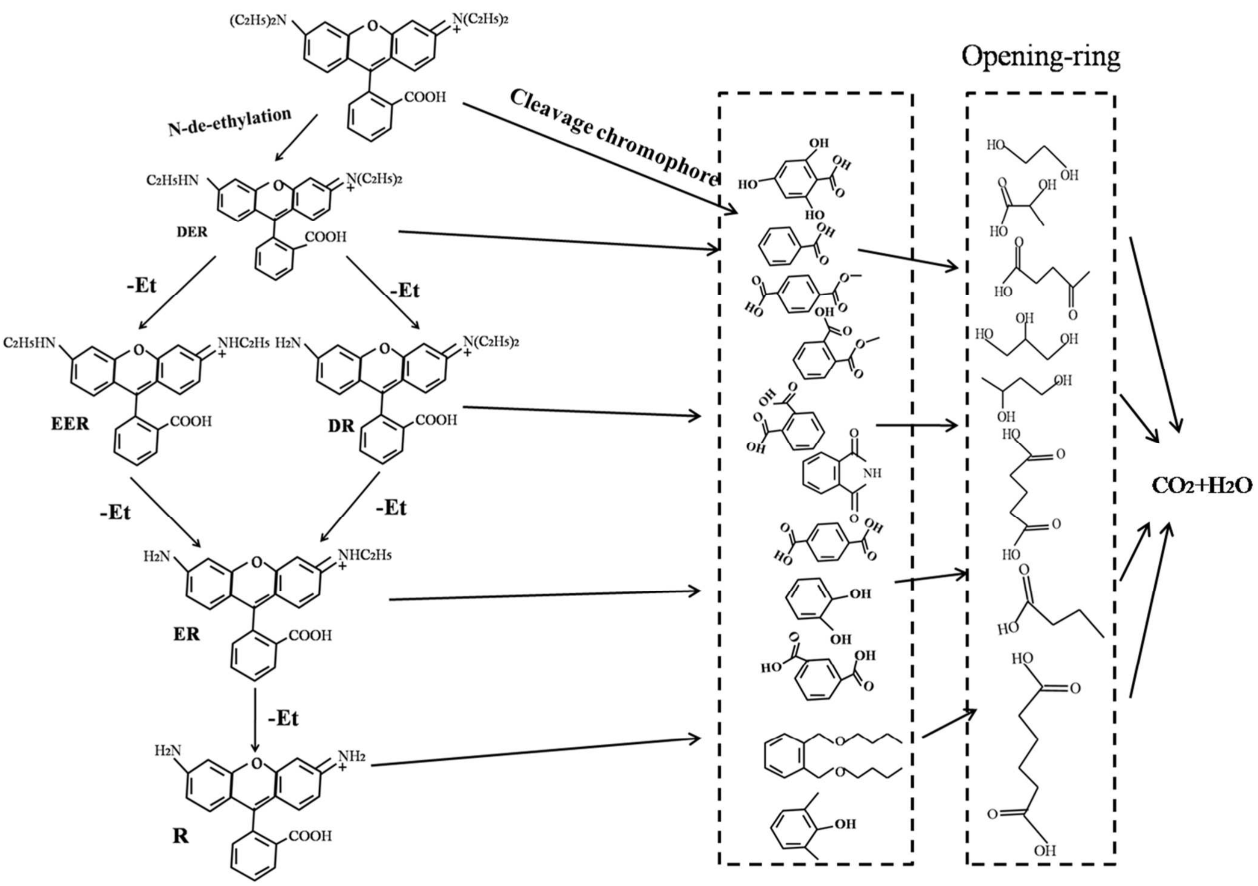

Fig. 10. Proposed pathway for the photocatalytic degradation of RhB dye under visible light.

View Article Online
DOI: 10.1039/C5RA16114B

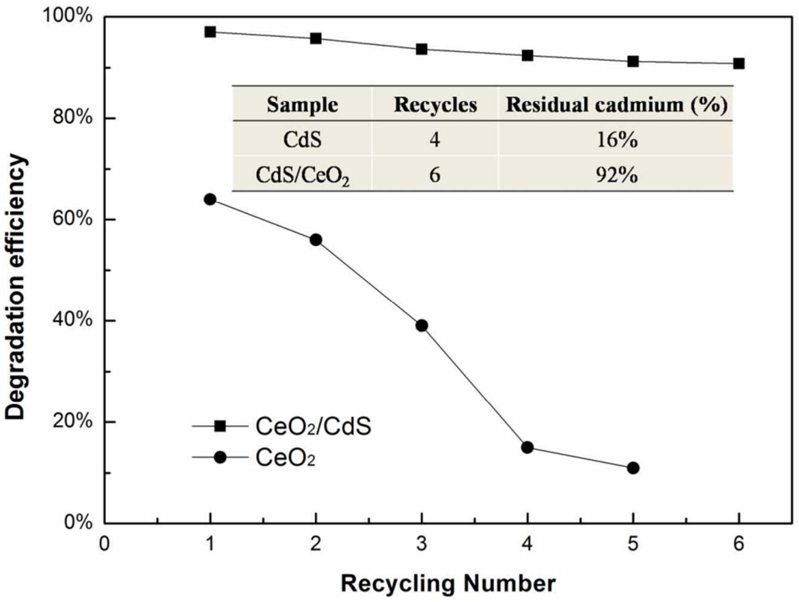

Sample	Recycles	Residual cadmium (%)
CdS	4	16%
CdS/CeO$_2$	6	92%

Fig. 11. Recycling test of CdS and CdS/CeO$_2$ and the ICP analysis of residual Cd^{2+} in the used photocatalysts.

View Article Online
DOI: 10.1039/C5RA16114B

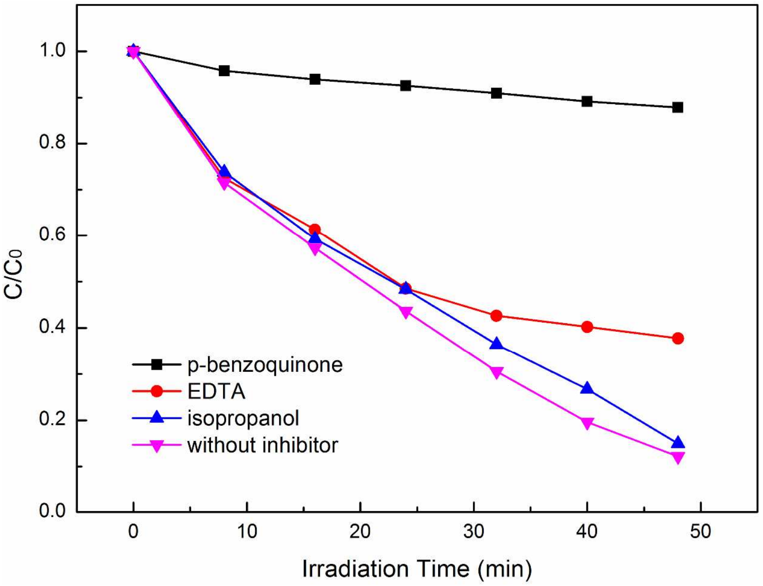

Fig. 12. Effect of radical scavenger on the degradation of RhB using EDTA scavenger for h^+, IPA for •OH and BQ for $O_2^{\bullet -}$, respectively.

View Article Online
DOI: 10.1039/C5RA16114B

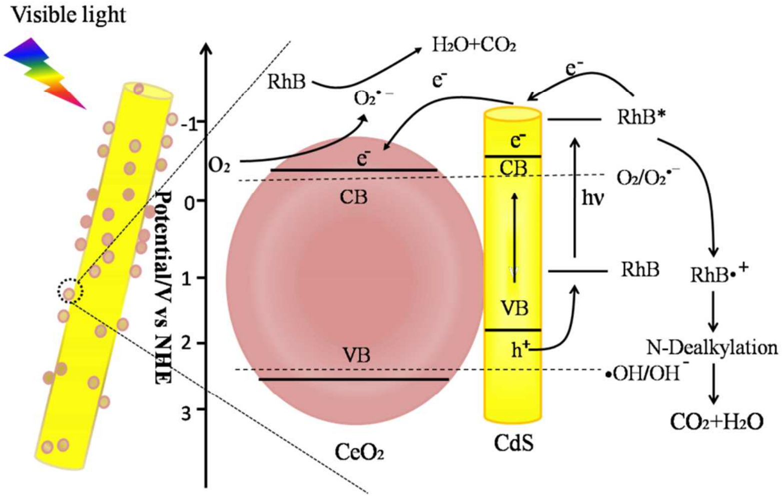

Fig. 13. Scheme diagram of the photocatalytic reaction of RhB on CdS/CeO_2 heterostructure.

View Article Online
DOI: 10.1039/C5RA16114B

Table 1 Textural property of photocatalysts.

Materials	BET surface area (m^2g^{-1})	Total pore volume (m^3g^{-1})	Average pore size (nm)
CdS	13.121	0.026	3.178
CeO_2	24.087	0.029	4.726
CdS/CeO_2	21.764	0.068	3.465

View Article Online
DOI: 10.1039/C5RA16114B

Table 2 RhB degradation rates of photocatalysts.

Materials	CdS	CeO_2	CdS/CeO_2 ($R_C = 20$)	CdS/CeO_2 ($R_C = 30$)	CdS/CeO_2 ($R_C = 10$)	CdS/CeO_2 ($R_C = 5$)
Degradation rate (min^{-1})	0.02089	0.00251	0.07003	0.04463	0.04182	0.03663